Solar UV radiation reduces the barrier function of human skin

Krysta Biniek, Kemal Levi, and Reinhold H. Dauskardt[1]

Department of Materials Science and Engineering, Stanford University, Stanford, CA 94305

Edited by John W. Hutchinson, Harvard University, Cambridge, MA, and approved August 31, 2012 (received for review April 25, 2012)

The ubiquitous presence of solar UV radiation in human life is essential for vitamin D production but also leads to skin photoaging, damage, and malignancies. Photoaging and skin cancer have been extensively studied, but the effects of UV on the critical mechanical barrier function of the outermost layer of the epidermis, the stratum corneum (SC), are not understood. The SC is the first line of defense against environmental exposures like solar UV radiation, and its effects on UV targets within the SC and subsequent alterations in the mechanical properties and related barrier function are unclear. Alteration of the SC's mechanical properties can lead to severe macroscopic skin damage such as chapping and cracking and associated inflammation, infection, scarring, and abnormal desquamation. Here, we show that UV exposure has dramatic effects on cell cohesion and mechanical integrity that are related to its effects on the SC's intercellular components, including intercellular lipids and corneodesmosomes. We found that, although the keratin-controlled stiffness remained surprisingly constant with UV exposure, the intercellular strength, strain, and cohesion decreased markedly. We further show that solar UV radiation poses a double threat to skin by both increasing the biomechanical driving force for damage while simultaneously decreasing the skin's natural ability to resist, compromising the critical barrier function of the skin.

The stratum corneum (SC), as the outermost layer of the epidermis, is the body's first line of defense against solar UV radiation. Solar UV radiation plays a dual role in human life: it is pivotal for vitamin D production (1) while also a potent and ubiquitous carcinogen responsible for much of the skin cancer in the human population (2). Although progress has been made in understanding the role of UV radiation in causing skin cancer (3), the role of solar UV radiation in altering the mechanical barrier function of the SC remains unknown.

The SC provides both critical mechanical protection and a controlled permeable barrier to the external environment. Although the SC is typically a highly efficient barrier, exposure to harsh conditions can alter its function, leading to severe skin damage such as chapping and cracking. Such damage can cause detrimental skin responses including inflammation and infection caused by compromised barrier function, scarring, and abnormal desquamation, and further aggravate the effects of skin disorders such as atopic dermatitis, ichthyosis vulgaris, and chronic xerosis (4–7).

UV radiation is divided into three main types based on wavelength: UVC radiation (200–280 nm) is predominately filtered by the ozone layer in the stratosphere, UVB radiation (280–320 nm) is mainly absorbed by the epidermis, and UVA radiation (320–400 nm) penetrates deeper into the dermis but interacts with both the SC and epidermis as well (8) (Fig. 1). The penetration of UV radiation into the skin can initiate detrimental photochemical reactions, causing both acute conditions such as erythema and chronic conditions such as photoaging, the main contributor to changes in skin's appearance with age (9), and skin cancers such as cutaneous malignant melanoma, basal cell carcinoma, and squamous cell carcinoma.

In the year 2000, excessive UV exposure caused the loss of ~1.5 million disability-adjusted life years (0.1% of the total global burden of disease) and 60,000 premature deaths globally (10). Climate change is expected to exacerbate this problem. Cooling of the stratosphere caused by the greenhouse effect is predicted to prolong the effect of ozone-depleting gases, which will increase levels of UV radiation reaching some parts of the Earth's surface. Climate change will also alter the distribution of clouds, which will, in turn, affect UV levels at the Earth's surface. Clothing choices and time spent outdoors will be influenced by higher ambient temperature, again potentially increasing UV exposure (11).

UVB radiation in particular can be very harmful. Recent in vivo studies have shown that UVB radiation affects epidermal morphology, including increasing the mean SC thickness (12), and disrupts the permeability barrier, causing morphological changes in SC lipids, increased transepidermal water loss, and decreased SC hydration (13, 14). Surprisingly, to our knowledge, no studies have explored how UV exposure affects the mechanical barrier function of SC. As a consequence, the relationship between UV exposure and the biomechanical behavior of human SC together with the biomechanical processes that lead to skin damage have not been established.

Here, we show the effect of UVB exposure on the cell cohesion and mechanical integrity of SC, as a function of UVB source (narrowband vs. broadband), dosage, and tissue depth. We then use thin-film biomechanical models to quantitatively predict the effect of UV exposure on damage processes in human skin. The study also lays the foundation for quantitatively determining the efficacy of UV inhibitors, e.g., sunscreens, at mitigating biomechanical UV damage.

Results

UVB Radiation Does Not Alter SC Stiffness. In vivo, the SC may be under considerable tensile stress; drying stress in particular can be significant and lead to damage that disrupts the barrier function (6, 15). We used microtension and bulge testing ($n = 3$ for each condition) to characterize the SC's stiffness, strength, and strain.

The stiffness remained surprisingly constant with increasing UVB exposure, even up to dosages of 800 J/cm^2, which corresponds to 60 continuous days of solar UVB radiation (Fig. 2*A*) (16). This very large dose is more than 14,000 times the average broadband UVB minimal erythema dose (17) and shows that the stiffness is largely insensitive to UV exposure. We selected UV dosages above those that are physiologically normal to amplify tissue responses and ensure we would observe easily detectable effects. It is therefore significant that we did not observe any effects on the SC stiffness. On the other hand, the specimens exhibited decreased fracture stress and a significant decrease in fracture strain with increasing UVB exposure (Fig. 2 *B* and *C*).

Author contributions: K.B., K.L., and R.H.D. designed research; K.B. and K.L. performed research; K.B., K.L., and R.H.D. analyzed data; and K.B. and R.H.D. wrote the paper.

The authors declare no conflict of interest.

This article is a PNAS Direct Submission.

Freely available online through the PNAS open access option.

[1]To whom correspondence should be addressed. E-mail: dauskardt@stanford.edu.

This article contains supporting information online at www.pnas.org/lookup/suppl/doi:10.1073/pnas.1206851109/-/DCSupplemental.

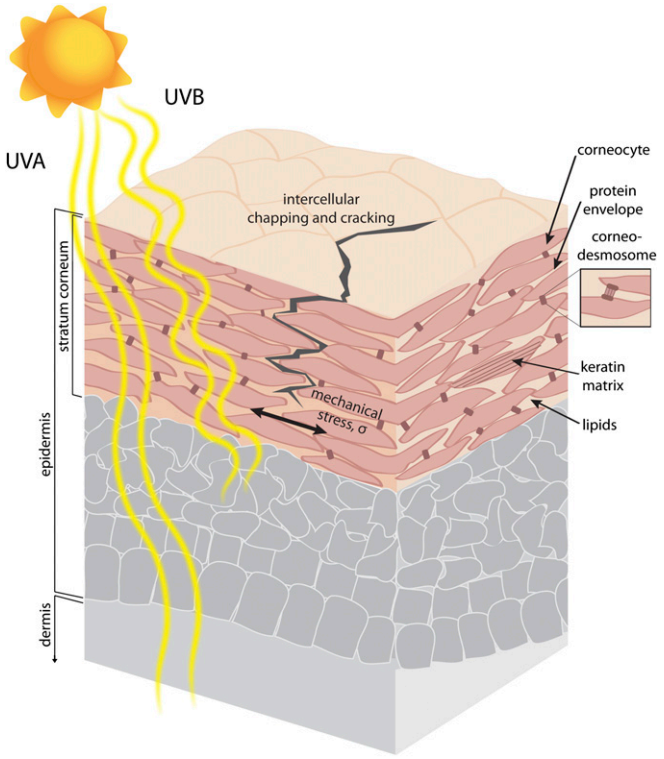

Fig. 1. Schematic of structure of human skin and penetration of different UV wavelengths. UVB penetrates mainly the epidermis.

Bulge testing was performed to study the biaxial biomechanical behavior of SC on a wet medium similar to its in vivo state. The SC specimens were pressurized with distilled water, causing them to deflect outward to form a balloon-like shape (Fig. 3*A*), from which the biaxial biomechanical behavior could be characterized. Unlike the stiffness measured using microtension, the SC biaxial stiffness significantly decreased with UV exposure (Fig. 3*B*). This difference in stiffness is related to the two testing methods: microtension testing was performed in air, whereas bulge testing was performed over water. Peak stress also significantly decreased with UV exposure (Fig. 3*C*).

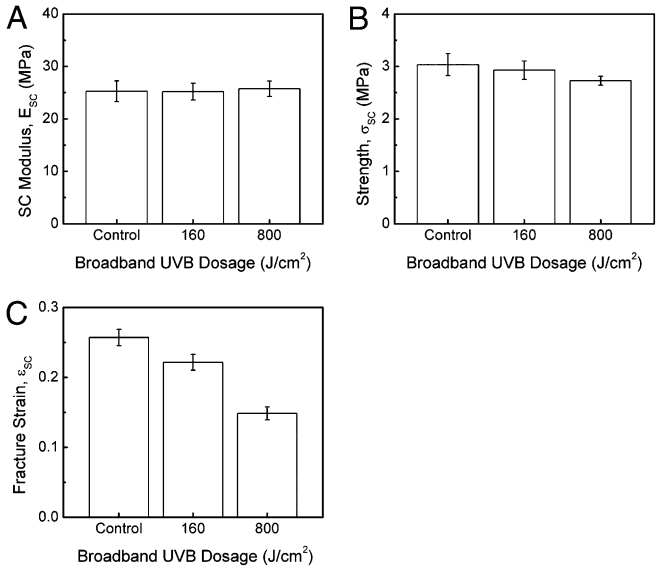

Fig. 2. (*A*) SC modulus, (*B*) SC fracture strength, and (*C*) SC fracture strain as a function of UV treatment for samples exposed to dosages of 0, 160, and 800 J/cm^2 UVB broadband radiation.

Intercellular Lipid Cohesion Decreases with UVB Exposure. A direct measure of cellular cohesion is given by the measurement of the tissue's delamination energy, or the energy required to separate intercellular boundaries (18). UVB-irradiated SC tissue was characterized using a double-cantilever beam (DCB) fracture mechanics specimen (Fig. 4*A*). An average of eight delamination energies were obtained per specimen for an average of $n = 24$ per test condition. To measure delamination energies through the thickness of the SC, successive DCB specimens were prepared from completely separated specimens by adhering new substrates onto each side of the previously tested specimen (Fig. 4*B*).

Intercellular delamination energy values, G_c, were measured for abdominal and breast specimens from donors ranging in age between 22 and 81 y with varying broadband and narrowband UVB exposure (Fig. 4*C*). As shown in previous studies (18), the delamination energy is the energy per unit area required to separate intercellular boundaries. With increasing UVB dosage, the specimens exhibited significantly lower delamination energies, suggesting decreased cohesion of the intercellular lipids with UV. This trend was seen across all tested body sites and age groups.

Cellular cohesion was also measured as a function of tissue depth (Fig. 4*D*). A very large decrease in cohesion with UV exposure at deeper layers was observed, revealing that the effect of UV exposure on skin is not limited to the upper SC and is in fact much more marked at deeper levels.

Structural Changes Occur in SC Lipids and Keratin Because of UVB Radiation. To interpret the effects of UV exposure on SC keratin and lipids, attenuated total reflectance Fourier transform infrared spectroscopy (ATR-FTIR) measurements were performed. The lipid content indicator, the ratio of the symmetric C—H_2 stretching peak to amide II peak, significantly decreased with increasing UVB exposure, suggesting that UV treatment reduces or modifies the lipid content of the SC (19) (Fig. 5*A*). The lipid fluidity indicator, given by the location of the antisymmetric and symmetric C—H_2 stretching peaks (20), initially increased and then decreased with increasing UVB exposure, indicating increased lipid fluidity near the surface of the SC (Fig. 5 *B* and *C*). The asymmetric and symmetric C—H_2 stretching frequencies decreased, however, with depth into the tissue, suggesting decreased lipid fluidity with tissue depth.

The amide I/amide II peak ratio increases with increasing UVB exposure, indicating an increase in hydration (21) (Fig. 5*D*). Furthermore, the amide II peak location significantly decreases with increasing UVB irradiation, suggesting that structural changes in the keratin take place (22) (Fig. 5*E*).

Discussion

The present study clearly reveals that UV radiation, although long known to cause DNA damage in skin (3, 23, 24), also causes significant changes in some of the mechanical properties of the SC. The delamination energy, which is the energy required to separate intercellular boundaries, the strength, and the strain to fracture all significantly decreased with UV exposure. Surprisingly, the stiffness, or Young's modulus, was largely unaffected for even large UV doses.

We expected these changes in mechanical properties to be related to the targets for UV within the SC. The SC's mechanical properties derive predominately from its main structural features: the SC has a composite structure consisting of heavily keratinized, disk-shaped corneocyte cells bound together by intercellular lipids and degraded desmosomal protein junctions, or corneodesmosomes (25).

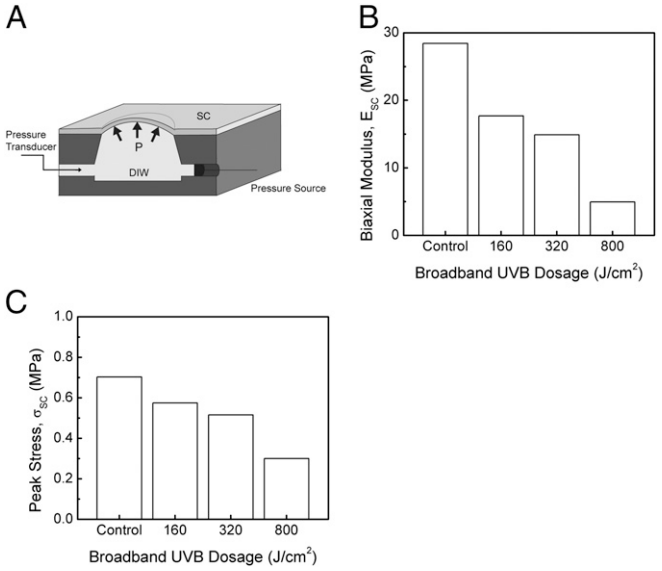

Fig. 3. (*A*) Bulge specimen geometry and testing schematic, (*B*) SC biaxial modulus, and (*C*) SC peak stress as a function of UV treatment for samples exposed to 160, 320, and 800 J/cm^2 UVB broadband radiation.

An initial surprising observation was that the stiffness was largely unaltered by even large UV doses. The stiffness of the SC is predominately controlled by the tissue's largest volume fraction, the intracellular keratin filament matrix within the cytoplasm of the corneocytes, which makes up ~80% of tissue volume (26) and 70% of the total dry weight mass of the SC (27). Hydrogen bonding between the polar side groups of individual keratin filaments causes a strong interaction between chains, which additionally complex with filaggrin to form a matrix (28). This keratin matrix lends the tissue rigidity, ensuring the stratum corneum maintains its dimensions and integrity in the presence of external mechanical stresses as well as internal osmotic stress (29). In addition to largely controlling the stiffness of the tissue, the keratin matrix is also a potential target for UV radiation.

It has been reported that UVA exposure increases the permeability of small polar alcohols through the SC while not affecting the permeability of larger, less polar alcohols. McAuliffe and Blank (30) argued that polar molecules pass through the keratin filaments of the SC, whereas the nonpolar molecules travel lipid pathways, indicating that UVA alters the protein structures of the SC. As proteins absorb UV radiation, it is reasonable to assume that structural changes in the proteins take place with UV exposure. Our ATR-FTIR data indicate that the decrease in the amide II peak location with UVB exposure corroborates that structural changes do take place in the keratin. Young's modulus, however, a measure of the keratin-controlled stiffness of the SC, remained constant even with large UV exposures, far above what would be encountered in a typical daily solar exposure. Our study suggests that the changes in keratin with UVB radiation do not influence the stiffness of the tissue, and we suspect the same may be true for UVA exposure. More recent research on the penetration of polar molecules through the SC has indicated that the route of penetration is in fact polar pores within the intercellular lipids (31), suggesting that, instead of affecting keratin, UV exposure causes alterations to the intercellular space.

Glycation, the reaction of reducing sugars with protein amino acids, is a possible explanation for the amide II peak shift. It occurs during intrinsic aging and in diabetic skin (32), and has also been shown to be enhanced by UV exposure (33). Glycation has been found to increase the cross-linking between keratin filaments, resulting in a stiffer tissue. We found that the stiffness of the SC remained constant with even large UV doses, suggesting we were not observing the effects of glycation.

The formation of reactive oxygen species (ROS) with UV exposure and their effect on proteins and lipids has also been extensively studied (34). ROS have been implicated in protein (35) and lipid (36) oxidation, which can alter tissue structure via cross-linking, fragmentation, etc. We expect ROS to be part of the damage processes in SC, although it was beyond the scope of this study to examine these reactions in detail.

In this study, the SC fracture strength and fracture strain decreased significantly with increasing UV exposure, indicating cellular cohesion, largely dominated by the intercellular lipids and corneodesmosomes, is reduced. Intercellular lipids, which form a "mortar" holding the corneocytes together, are another potential target for damage by UV radiation. Intercellular lipids make up 20% of total tissue volume, or about 15% of the total dry weight of the SC, and are arranged in lamellar sheets, which consist of bilayers of ceramides, cholesterol, and fatty acids together with small amounts of phospholipids and glucosylceramides (37).

The cellular cohesion is more directly determined by the measurement of the tissue's delamination energy. Our previous research clearly identified that delamination of SC is intercellular: the removal of mobile lipids in SC increased the intercellular delamination energy as covalently bound lipids were brought into closer proximity (18, 38, 39). Thus, the marked decrease in intercellular delamination energy with increasing UV exposure indicates UV radiation causes a significant decrease in cellular cohesion and thus an alteration of intercellular lipid or corneodesmosome

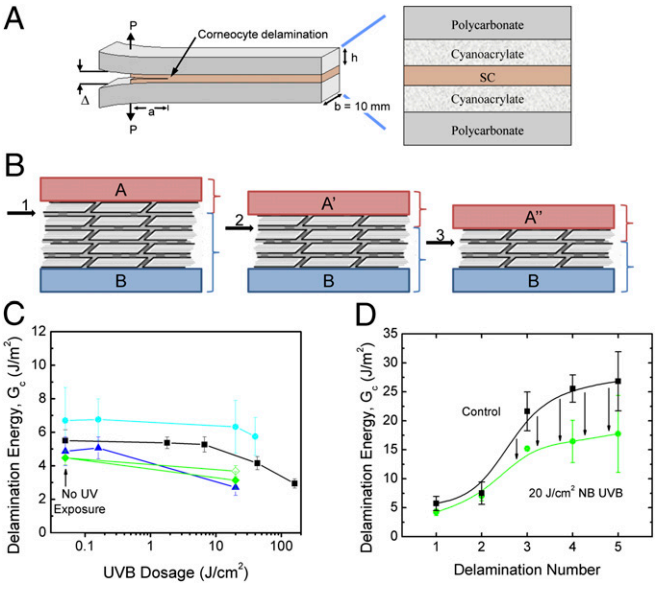

Fig. 4. (*A*) Fracture mechanics specimen geometry and testing schematic. DCB geometry illustrating relevant loading parameters (P, Δ), delamination extension as measured from loading axis points (*a*) and relevant specimen dimensions (b = 10 mm, h = 2.88 mm, length = 40 mm). (*B*) Illustration of graded properties measurement method in which initially tested DCB substrate (B) is adhered to new substrate (A′) to form new DCB specimen and subsequently tested. The original substrates are tested again in this manner using new substrates each time (A″), etc., until the desired number of delaminations is completed. (*C*) SC delamination energy as a function of UV treatment for abdomen or breast specimens from donors ranging in age from 22 to 81 y exposed to varying dosages of broadband and narrowband UVB radiation. Note the log scale used for UVB dosage. (*D*) Delamination energy values for DCB tests performed on untreated SC and SC exposed to a dosage of 20 J/cm^2 narrowband UVB radiation versus number of delaminations.

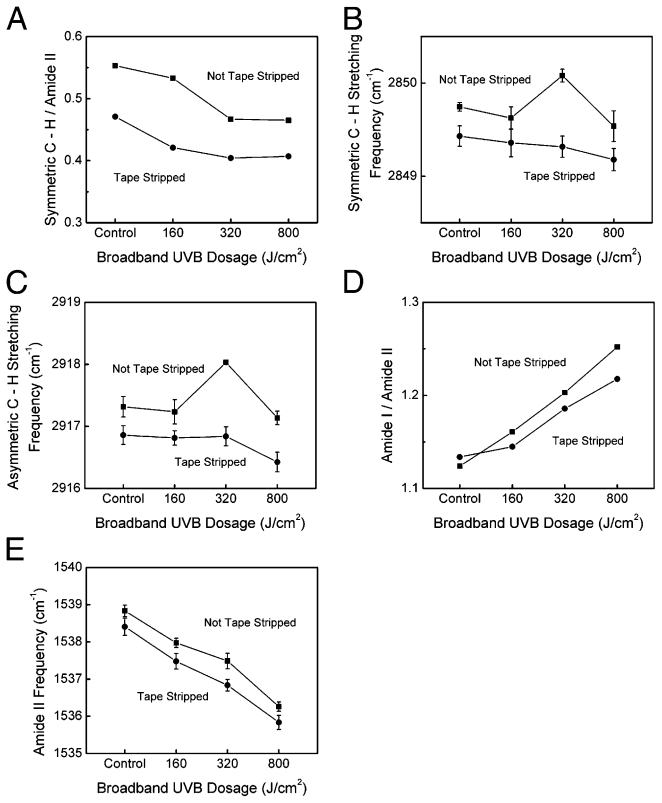

Fig. 5. (*A*) The lipid content indicator, given as the ratio of the symmetric C—H stretching peak to amide II peak, as a function of broadband UVB dosage. (*B*) Symmetric and (*C*) asymmetric C—H stretching frequency as a function of broadband UVB dosage for non–tape-stripped and tape-stripped samples. (*D*) Ratio of amide I to amide II peak heights as a function of broadband UVB dosage. (*E*) Amide II peak location as a function of broadband UVB dosage.

structure. Furthermore, these UV-induced alterations are prevalent throughout the depth of the SC and are more pronounced away from the upper, superficial layers.

In addition to intercellular lipid contributions to SC integrity, the corneodesmosome protein linkages between cells are known to play a critical role in SC cohesion. Previous delamination testing on human SC revealed a gradient in SC intercellular cohesion with progressively weaker bonding from the lower layers toward the more superficial layers of the SC. These graded delamination tests also determined that the first delamination occurs in the first few outer layers of the SC, where the concentration of corneodesmosomes is relatively low, with subsequent delaminations occurring at progressively deeper layers (39). The decrease in delamination energy in the upper layers of the SC with UV exposure can thus be attributed mainly to intercellular lipids and indicates that the cohesion of intercellular lipids decreases with UV exposure. The more marked decrease in cellular cohesion with depth into the tissue indicates that corneodesmosomes are altered by UV exposure.

Corneodesmosomes are critical to desquamation, an important protective mechanism by which the SC is completely turned over in 2–4 wk. The progressive degradation of corneodesmosomes toward the outer skin surface decreases cellular cohesion and facilitates cell detachment. The damage of corneodesmosomes by UV exposure is expected to alter the natural desquamation process, potentially leading to longer-term barrier disruption. Future research should examine how the initial damage from UV exposure affects subsequent generations of SC.

Comparing the present results to other organic films exposed to UV radiation, we found that the fracture energy of polysiloxane-coated poly(methyl methacrylate) (PMMA) decreased by ∼30% with exposure to simulated solar radiation because of chain scission in the PMMA substrate (40), whereas the delamination energy of organosilicate films increased with UV radiation because of formation of cross-linking Si—O—Si bonds (41). Thus, the response of a thin-film material to UV exposure is highly dependent upon the specific material's bonding and structure.

Surprisingly, the biaxial stiffness obtained using the bulge test significantly decreased with increasing UV exposure. Although Young's modulus of the tissue determined using uniaxial tensile testing remained constant, the bulge test is a fundamentally different type of test: the tissue is stretched over water similar to its in vivo state, allowing water ingress. A decrease in SC biaxial stiffness indicates that the tissue becomes more hydrophilic with UV exposure, resulting in increased water uptake and increased hydration. The increase in water absorption indicates that the intercellular lipids are modified by UV exposure.

The structural integrity of keratin and intercellular lipids plays an important role in the hydration characteristics of SC, and intercellular lipids have been identified as the primary barrier to water permeability through the SC layer (25, 42). With only tightly bound water present in dry environments [<20% relative humidity (RH)], SC has a dense, semicrystalline structure. There is a strong interaction between the keratin chains because of hydrogen bonding between the polar-side groups of the chains (43, 44), and the intercellular lipids are closely packed and rigid. As the tissue hydrates, the hydrogen bonding between the keratin chains is disrupted, allowing them to be less constrained and move more easily relative to each other while being strained (43, 45). In the case of the lipids, increasing water presence reduces the intermolecular forces between the intercellular lipids and loosens their packing, causing them to become more fluid and permeable (45). As a result, the tissue becomes weaker and less stiff with increasing hydration. A lower biaxial modulus therefore indicates the tissue has become more hydrophilic with UV exposure, suggesting an alteration in lipid structure.

To limit variability between specimens, all biomechanical testing was performed on SC obtained from female Caucasian donors. The donors ranged in age from 22 to 81 y, and SC was selected predominately from the abdomen and one sample from the breast, which may have had a different sun exposure history. Future research should examine how such factors as sex, race, age, anatomical site, and history of sun exposure and tobacco use alter the response of tissue to UV exposure. For example, the need to balance protection from sunburn and skin cancer with the ability to produce vitamin D has caused the evolution of skin pigmentation through natural selection for optimization to the levels of UV radiation at a given latitude (46). Variations in skin pigmentations may therefore be expected to have a significant impact on UV-induced alterations to the mechanical barrier function of skin.

Based on the biomechanical model we have developed to predict the onset of SC damage, we can make some predictions regarding the effects of UV exposure. The driving force for crack propagation for various cracking configurations can be quantified in terms of the strain energy release rate, G (47):

$$G = \frac{Z\sigma_{SC}^2 h_{SC}}{E_{SC}} \quad [1]$$

where σ_{SC} is the SC drying stress, h_{SC} is the SC thickness, E_{SC} is the biaxial SC modulus, and Z is a nondimensional parameter for the specific cracking configuration ($Z = 3.95$ for surface cracks, 1.98 for channel cracking, and 0.50 for delamination) (Table S1). Note that this formulation assumes that the SC is a linear elastic thin film on an elastic substrate, which is accurate for the low

strains, hydration conditions, and timescales important for dry skin damage processes. The viscoelastic nature of the epidermal and dermal substrate layers will likely result in a greater mechanical driving force for skin damage.

Cracking and chapping will develop in the SC during drying when the value of G exceeds the intercellular delamination energy, G_c, which provides a measure of the SC's natural resistance to damage. Chapping and cracking can lead to serious adverse skin responses such as inflammation and infection caused by the SC's impaired barrier function (4–7). We have shown that the biaxial stiffness, E_{SC}, in Eq. **1** decreases with UV exposure, leading to an increase in the crack driving force, G. The biaxial stiffness is a more appropriate parameter than the uniaxial stiffness in this instance because the measure of the biaxial stiffness, the bulge test, is performed under conditions that simulate the in vivo environment. For a conservative measure of the crack driving force G, and to enable comparison with the intercellular cohesion, G_C, measured at 30% RH, the stiffness was assumed to be constant at 200 MPa, a typical value for the tissue at 30% RH (15). The biaxial drying stress, σ_{SC}, was characterized from the curvature of an elastic substrate onto which the SC has been adhered (15, 48). The drying stress significantly increased with UV radiation, and the crack driving force, G, scales with the biaxial drying stress, σ_{SC}, to the power of 2 in Eq. **1**. Thus, the crack driving force, G, is predicted to significantly increase with UV exposure.

The tissue's intercellular delamination energy, G_c, decreases with UV exposure, suggesting that UV radiation poses a double threat to skin: it both increases the crack driving force while simultaneously decreasing the skin's natural ability to resist (Fig. 6). It should be noted, however, that our model predicts the onset of damage to occur at a large broadband UVB dose of 25 J/cm^2, which corresponds to about 2 d of solar exposure. The SC is therefore inherently resistant to even relatively severe UV exposure.

We thus show that UV exposure has dramatic effects on SC cell cohesion and mechanical integrity that are related to its effects on SC intercellular lipids and corneodesmosomes. Although ATR-FTIR indicated structural changes in keratin occur with UVB exposure, the results of microtension, bulge, and double cantilever beam testing indicate that the intercellular lipids and corneodesmosomes are the primary tissue components affected by UVB radiation. The alteration of the SC intercellular space has dramatic implications for the SC's barrier properties and mechanical integrity and highlights the need for effective protection from UV. The protection level of UV inhibitors such as sunscreens is quantified by its sun protection factor, the ability to protect against sunburn, and largely disregards any alterations in the biomechanical barrier function of SC (49). This study also lays the foundation for investigation of the efficacy of UV inhibitors such as sunscreens at preventing UV damage to the biomechanical barrier function of SC.

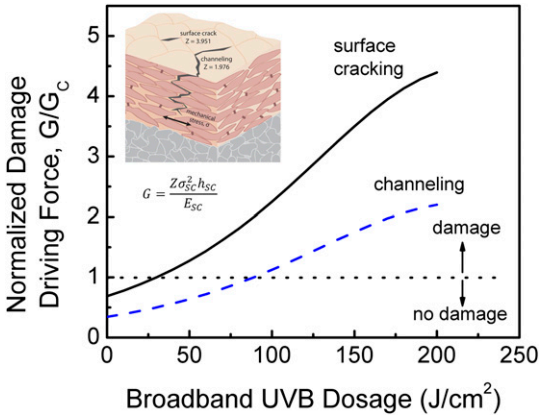

Fig. 6. The normalized driving force for SC damage, given as the ratio of G/G_c, as a function of broadband UVB dosage for surface cracking and channeling configurations. Surface cracks nucleate from a given size flaw and propagate downward toward the SC/epidermis interface. Channel cracks propagate in the plane of the SC. G is the strain energy release rate, or crack driving force, of UV-exposed tissue, and G_c is the intercellular delamination energy, a measure of the tissue's natural resistance to damage. The crack driving force significantly increases with UV exposure while the natural resistance to damage decreases, leading to increased damage and impaired biomechanical function.

Materials and Methods

Tissue Preparation. Human cadaver SC was acquired from the abdomen and breast of Caucasian female donors between the ages of 22 and 81 y. Frozen cadaver tissue was stored at −80 °C until processing. Single donor tissue specimens were used for comparative tests to reduce variability within the test sequences. Epidermal tissue was separated from the dermis by immersion in a 35 °C water bath for 10 min followed by a 1 min soak at 60 °C, and then mechanical separation from the dermis using a flat-tipped spatula. SC was subsequently detached from underlying epidermis by floating the tissue in a trypsin enzymatic digest solution [0.1% (wt/wt) in 0.05 M, pH 7.9 Tris buffer] at 35 °C for 120 min. The tissue was then floated on water and the epidermis was gently brushed away using a Q-tip until a clear sheet of SC was obtained. The SC was then rinsed and allowed to dry on filter paper (grade 595 general-purpose filter paper; Schleicher and Schuell MicroScience), and then removed and stored in a low-humidity chamber (~10–20% RH) at an ambient temperature of ~18–23 °C.

Specimens were equilibrated in an environmental chamber (LH-6 Humidity Chamber; Associated Environmental Systems) for 24 h before UV exposure and specimen fabrication. The specimens were then exposed to different doses of broadband and narrowband UVB radiation using phototherapy lamps (SolRx 100; SolarC Sytems) or Pen-Ray UV lamps (Pen-Ray Lamp; UVP) (Fig. S1). The SolRx phototherapy device uses UVB narrowband bulbs (PL-S 9W/01/2P; Philips) emitting radiation with wavelengths between 305 and 315 nm with a peak at 311 nm and UVB broadband bulbs (PL-S 9W/12/2P; Philips) emitting radiation with wavelengths of 270–400 nm with a peak at 311 nm. The Pen-Ray UVB lamp emits broadband radiation between 280 and 375 nm, with the principal emission at 302 nm. The broadband and narrowband UVB lamps had an average intensity of 1.4 and 1.2 mW/cm^2, respectively. A dosage of 160 J/cm^2 of broadband or narrowband UVB radiation, for example, thus required an exposure time of 31 h, 45 min, or 37 h, 2 min, respectively.

Biomechanical Testing. We performed microtension, bulge, and double cantilever beam experiments as previously described (18, 50) and briefly reviewed here.

Microtension experiments were performed using a tensile testing apparatus (Bionix 200; MTS Systems Corporation) equipped with a 44.48 N load cell to study the uniaxial biomechanical behavior of the tissue. The specimens were trimmed to 25 × 6 mm and mounted onto opposing grips with a 10-mm-long gauge length. Specimens were tested to failure in all cases with an initial strain rate of 0.01 s^{-1}.

Bulge testing was conducted using a Plexiglas unit encasing a drilled cavity with two channels, which were filled with distilled water as the pressure medium. UVB-irradiated SC specimens (5 × 5 mm) were clamped onto the orifice of the cavity, and one side of the specimen was exposed to distilled water for 1 h before testing. The SC was bulged outward with distilled water at a constant medium flow rate of 0.0445 μL s^{-1}, and the pressure inside the system was measured by a pressure transducer. Experiments were performed at a constant temperature and RH condition, i.e., at 23 °C and 25% RH. To determine the biaxial stress and strain in the SC, the pressurized tissue was modeled as a section of a thin-walled spherical pressure vessel having uniform equal biaxial stress and curvature.

To form DCB specimens, UV-irradiated SC was adhered between two elastic substrates of polycarbonate with cyanoacrylate adhesive. To enable the use of linear elastic fracture mechanics to determine the strain energy release rates, substrate dimensions of 40 × 10 × 3 mm^3 were chosen to ensure purely elastic deformation of the substrates during testing. The specimens were mounted at the SC-free end via loading tabs in an adhesion test system with a computer-controlled DC servoelectric actuator operated in displacement control to propagate a debond through the SC layer. Tests were performed at a constant displacement rate of 2 μm/s. To perform graded delamination tests, DCB specimens were fabricated and tested as described above. After testing the new specimen, the substrate from the original delamination specimen would again be adhered to another new substrate to delaminate the remaining SC layer.

ATR-FTIR. We performed ATR-FTIR using a Vertex 70 FTIR spectrometer (Bruker Optics) equipped with a deuterated triglycine sulfate detector and a micro-ATR (A529-P MIRacle) accessory supporting a ZnSe crystal. Data collection and spectral calculations were performed using OPUS (version 5.5) software. All spectra (2 cm^{-1} resolution) were obtained in the frequency range of 4,000–750 cm^{-1} and normalized by the amide I peak at ~1,650 cm^{-1} largely because of carbon-oxygen (C=O) stretching with a small contribution from nitrogen-hydrogen (N—H) bend. Second derivative of the spectra was used to identify peak positions. Studies in the literature typically look at the effect of UVB on the surface of the SC (22). The SC surface can give misleading results, however, because of possible surface contamination. Tape stripping was used to remove any potential surface contamination. ATR-FTIR measurements of both tape-stripped and non-tape-stripped SC specimens were obtained for comparison.

Statistical Analysis. Microtension and bulge data, as well as delamination energies measured as a function of conditioning, are presented as mean values $\pm$ 1.96 $\times$ the SEM in which the mean values reported are expected to fall within these bounds with 95% confidence. On average, $n = 3$ for each test condition. For double cantilever beam testing, an average of eight delamination energies were obtained per specimen, yielding on average $n = 24$ per test condition. Values were compared using the Wilcoxon signed-ranks test for independent samples. The confidence interval was set at 95%. In the ATR-FTIR study, four scans were made at different regions of the specimens to confirm the trends. The absorbances and peak heights are reported as mean $\pm$ SD of four samples.

ACKNOWLEDGMENTS. This work was supported by the US Department of Energy, under Contract DE-FG02-07ER46391. K.B. was supported by a National Science Foundation Fellowship.

1. Holick MF (2004) Sunlight and vitamin D for bone health and prevention of autoimmune diseases, cancers, and cardiovascular disease. *Am J Clin Nutr* 80 (6, Suppl)1678S–1688S.
2. Armstrong BK, Kricker A (2001) The epidemiology of UV induced skin cancer. *J Photochem Photobiol B* 63:8–18.
3. Brash DE, et al. (1991) A role for sunlight in skin cancer: UV-induced p53 mutations in squamous cell carcinoma. *Proc Natl Acad Sci USA* 88:10124–10128.
4. Gaul LE, Underwood GB (1952) Relation of dew point and barometric pressure to chapping of normal skin. *J Invest Dermatol* 19:9–19.
5. Harding CR, et al. (2003) The cornified cell envelope: An important marker of stratum corneum maturation in healthy and dry skin. *Int J Cosmet Sci* 25:157–167.
6. Edlich RF, Carl BA (1998) Predicting scar formation: From ritual practice (Langer's lines) to scientific discipline (static and dynamic skin tensions). *J Emerg Med* 16: 759–760.
7. Larson EL, et al. (1998) Changes in bacterial flora associated with skin damage on hands of health care personnel. *Am J Infect Control* 26:513–521.
8. Hussein MR (2005) Ultraviolet radiation and skin cancer: Molecular mechanisms. *J Cutan Pathol* 32:191–205.
9. Gilchrest BA (1989) Skin aging and photoaging: An overview. *J Am Acad Dermatol* 21: 610–613.
10. Lucas RM, McMichael AJ, Armstrong BK, Smith WT (2008) Estimating the global disease burden due to ultraviolet radiation exposure. *Int J Epidemiol* 37:654–667.
11. Parry ML, Canziani OF, Palutikof JP, van der Linden PJ, Hanson CE, eds (2007) Climate change 2007: Working group II: Impacts, adaption and vulnerability. *Fourth Assessment Report of the Intergovernmental Panel on Climate Change* (Cambridge Univ Press, Cambridge, UK).
12. Pearse AD, Gaskell SA, Marks R (1987) Epidermal changes in human skin following irradiation with either UVB or UVA. *J Invest Dermatol* 88:83–87.
13. Kambayashi H, Odake Y, Takada K, Funasaka Y, Ichihashi M (2003) Involvement of changes in stratum corneum keratin in wrinkle formation by chronic ultraviolet irradiation in hairless mice. *Exp Dermatol* 12(Suppl 2):22–27.
14. Meguro S, Arai Y, Masukawa K, Uie K, Tokimitsu I (1999) Stratum corneum lipid abnormalities in UVB-irradiated skin. *Photochem Photobiol* 69:317–321.
15. Levi K, Weber RJ, Do JQ, Dauskardt RH (2010) Drying stress and damage processes in human stratum corneum. *Int J Cosmet Sci* 32:276–293.
16. ASTM International (2008) Standard tables for reference solar spectral irradiances, direct normal and hemispherical on 37° tilted surface. *ASTM Standard G173* (ASTM International, West Conshohocken, PA).
17. van Weelden H, De La Faille HB, Young E, van der Leun JC (1988) A new development in UVB phototherapy of psoriasis. *Br J Dermatol* 119:11–19.
18. Wu KS, van Osdol WW, Dauskardt RH (2006) Mechanical properties of human stratum corneum: Effects of temperature, hydration, and chemical treatment. *Biomaterials* 27:785–795.
19. Hatanaka T, Shimoyama M, Sugibayashi K, Morimoto Y (1993) Effect of vehicle on the skin permeability of drugs: Polyethylene glycol 400-water and ethanol-water binary solvents. *J Control Release* 23:247–260.
20. Casal HL, Mantsch HH (1984) Polymorphic phase behaviour of phospholipid membranes studied by infrared spectroscopy. *Biochim Biophys Acta* 779:381–401.
21. Lucassen G (1998) Band analysis of hydrated human skin stratum corneum attenuated total reflectance Fourier transform infrared spectra in vivo. *J Biomed Opt* 3:267.
22. Barry BW, Edwards HGM, Williams AC (1992) Fourier transform Raman and infrared vibrational study of human skin: Assignment of spectral bands. *J Raman Spectrosc* 23: 641–645.
23. Kielbassa C, Roza L, Epe B (1997) Wavelength dependence of oxidative DNA damage induced by UV and visible light. *Carcinogenesis* 18:811–816.
24. de Gruijl FR, van Kranen HJ, Mullenders LHF (2001) UV-induced DNA damage, repair, mutations and oncogenic pathways in skin cancer. *J Photochem Photobiol B* 63:19–27.
25. Elias PM, Grayson S, Lampe MA, Williams ML, Brown BE (1983) The intercorneocyte space. *Stratum Corneum*, eds Marks R, Plewig G (Springer, Berlin), pp 53–67.
26. Marjukka Suhonen T, Bouwstra JA, Urtti A (1999) Chemical enhancement of percutaneous absorption in relation to stratum corneum structural alterations. *J Control Release* 59:149–161.
27. Steinert PM, et al. (1985) Amino acid sequences of mouse and human epidermal type II keratins of Mr 67,000 provide a systematic basis for the structural and functional diversity of the end domains of keratin intermediate filament subunits. *J Biol Chem* 260:7142–7149.
28. Steinert PM (1983) Epidermal keratin: Filaments and matrix. *Stratum Corneum*, eds Marks R, Plewig G (Springer, Berlin), pp 25–38.
29. Norlén L, Al-Amoudi A (2004) Stratum corneum keratin structure, function, and formation: The cubic rod-packing and membrane templating model. *J Invest Dermatol* 123:715–732.
30. McAuliffe DJ, Blank IH (1991) Effects of UVA (320-400 nm) on the barrier characteristics of the skin. *J Invest Dermatol* 96:758–762.
31. Menon GK, Elias PM (1997) Morphologic basis for a pore-pathway in mammalian stratum corneum. *Skin Pharmacol* 10(5–6):235–246.
32. Bucala R, Cerami A (1992) Advanced glycosylation: Chemistry, biology, and implications for diabetes and aging. *Adv Pharmacol* 23:1–34.
33. Jeanmaire C, Danoux L, Pauly G (2001) Glycation during human dermal intrinsic and actinic ageing: An in vivo and in vitro model study. *Br J Dermatol* 145:10–18.
34. Scharffetter-Kochanek K, et al. (1997) UV-induced reactive oxygen species in photocarcinogenesis and photoaging. *Biol Chem* 378:1247–1257.
35. Stadtman ER (1992) Protein oxidation and aging. *Science* 257:1220–1224.
36. Gutteridge JM (1995) Lipid peroxidation and antioxidants as biomarkers of tissue damage. *Clin Chem* 41:1819–1828.
37. Harding CR (2004) The stratum corneum: Structure and function in health and disease. *Dermatol Ther* 17(Suppl 1):6–15.
38. Wu K, Li J, Ananthapadmanabhan K, Dauskardt R (2007) Time-dependant intercellular delamination of human stratum corneum. *J Mater Sci* 42:8986–8994.
39. Wu KS, Stefik MM, Ananthapadmanabhan KP, Dauskardt RH (2006) Graded delamination behavior of human stratum corneum. *Biomaterials* 27:5861–5870.
40. Kamer A, Larson-Smith K, Pingree LSC, Dauskardt RH (2011) Adhesion and degradation of hard coatings on poly (methyl methacrylate) substrates. *Thin Solid Films* 519:1907–1913.
41. Kim T-S, et al. (2008) Tuning depth profiles of organosilicate films with ultraviolet curing. *J Appl Phys* 104(7):074113-1–074113-6.
42. Fartasch M (1997) Epidermal barrier in disorders of the skin. *Microsc Res Tech* 38: 361–372.
43. Takahashi M, Kawasaki K, Tanaka M, Ohta S, Tsuda Y (1981) The mechanism of stratum corneum plasticization with water. *Bioengineering and the Skin*, eds Marks RM, Payne PA (MTP Press Ltd, Lancaster, UK), pp 67–73.
44. Jokura Y, Ishikawa S, Tokuda H, Imokawa G (1995) *Molecular Analysis of Elastic Properties of the Stratum Corneum by Solid-State ^{13}C-Nuclear Magnetic Resonance Spectroscopy* (Nature Publishing Group, New York), p 7.
45. Barry BW (1988) Action of skin penetration enhancers—the Lipid Protein Partitioning theory. *Int J Cosmet Sci* 10:281–293.
46. Jablonski NG, Chaplin G (2010) Colloquium paper: Human skin pigmentation as an adaptation to UV radiation. *Proc Natl Acad Sci USA* 107(Suppl 2):8962–8968.
47. Hutchinson JW, Suo Z (1991) Mixed mode cracking in layered materials. *Adv Appl Mech* 29:63–191.
48. Levi K, et al. (2010) Emollient molecule effects on the drying stresses in human stratum corneum. *Br J Dermatol* 163:695–703.
49. *Federal Register* 76 (2011), Labeling and effectiveness testing; sunscreen drug products for over-the-counter human use, pp 35620–35665.
50. Jia R, et al. (2011) Effect of cation contamination and hydrated pressure loading on the mechanical properties of proton exchange membranes. *J Power Sources* 196: 3803–3809.